Hindawi
Complexity
Volume 2020, Article ID 4812657, 15 pages
https://doi.org/10.1155/2020/4812657

Research Article

Adaptive Variable Parameter Impedance Control for Apple Harvesting Robot Compliant Picking

Ji Wei,[1] **Ding Yi**,[1] **Xu Bo**,[1] **Chen Guangyu**,[1] **and Zhao Dean**[1,2]

[1]*School of Electrical and Information Engineering, Jiangsu University, Zhenjiang 212013, China*
[2]*High-tech Key Laboratory of Agricultural Equipment and Intelligence of Jiangsu Province, Jiangsu University, Zhenjiang 212013, China*

Correspondence should be addressed to Ji Wei; jiwei@ujs.edu.cn

Received 21 October 2019; Revised 31 December 2019; Accepted 9 March 2020; Published 4 April 2020

Academic Editor: Alex Alexandridis

In order to reduce the damage of apple harvesting robot to fruits and achieve compliant picking, an adaptive variable parameter impedance control method for apple harvesting robot compliant picking is proposed in this paper. Firstly, the Burgers viscoelastic model is used to characterize the rheological properties of apples and study the variation of mechanical properties of apple grasping at different speeds. Then, a force-based impedance control system is designed. On this basis, aiming at the influence of impedance controller parameters on contact force, three impedance parameters self-tuning functions are constructed to complete the design of an improved force-based impedance control system based on the hyperbolic secant function. The simulation and experimental results show that the proposed control makes the desired force smoother, and its overshoot is about 2.3%. The response speed is faster, and the adjustment time of contact force is shorter of about 0.48 s. The contact force overshoot is about 2%, which is 37.5% less than that of the traditional force-based impedance control. This research improves the control performance for apple harvesting robot compliant picking.

1. Introduction

With the development of modern agriculture, harvesting robot is becoming an important area of robot application. The picking operation of harvesting robot is the key link to realize the automation and mechanization of fresh fruit and vegetable harvesting [1]. In the picking process, interaction control between the robot end-effector and the fruit is crucial to reduce the mechanical damage of fruit and successfully picking, since the robot end-effector has to contact and operate on the surface of fruit.

In order to solve the problem of rapid compliant picking, many scholars have conducted a lot of research studies, and many studies have applied impedance control to it. For example, based on the optimal control theory, the set value of the internal impedance control layer was calculated by using the external admittance control layer, and the gain of the impact model was optimized to achieve the control performance with estimated error [2]. To realize the flexible adjustment of force and position of the manipulator under high-speed clamping and achieve good tracking effect, a robust impedance control method was proposed [3]. The grasping constraint relationship between the end-effector of robot and the fruit was equivalent to a second-order impedance-admittance model. The deviation between the desired grasping force and the contact force of fruit was used as the input of the impedance controller, and the reference trajectory was corrected to form an impedance tracking control for the grasping force of the end-effector which was suitable for double-fingered grasping [4]. In free space and constraint space, position-based impedance control and force tracking control were used, respectively. A fuzzy observer was introduced to switch the two control stages. The precise position tracking of the manipulator in free space was realized, and the grasping force can be tracked accurately through a smooth transition to the constraint space [5]. There were also other studies, such as the sliding signal detector for calculating the sliding amplitude and the

grasping force setpoint generator acting on the output of the detector. The detector combined the force adjustment with sliding detection closely to adjust the grasping force accurately and achieved the purpose of grasping objects [6]. In order to study the effect of fruit-finger interaction parameters on the probability of thumb-index finger stability grip, a logistic regression model was used to reasonably predict the probability of two-finger stability grip and to analyze the grasp of two-finger force of picking robot [7]. Ba et al. designed the flexibility enhancement controller with feedforward compensator and rearranged the dynamic flexibility composition of the internal and external HDU control loops, thus improving the control accuracy. Semini et al. studied the problem of active impedance to improve the stability and usefulness of legged robots. These research studies demonstrated the advantages and the potential of active impedance and torque-controlled robots within a series of new experiments.

To summarize, previous studies have been carried on the different aspect analysis to the robot grasping force control. However, the abovementioned research studies did not consider the influence of the mechanical characteristics of the object on grasping control and did not optimize the control model aiming at the online adjusting ability of the robot grasping object, which cannot adapt to the complex environment of apple fruit grasping. Thus, the objective of this study is to improve the traditional impedance control for apple harvesting robot end-effector and meet with the requirements of compliant picking. The study establishes the viscoelastic characteristics of fruit and analyzes the law of deformation in the process of grasping. On this basis, an improved force-based impedance control system is designed. The time-varying functions of impedance controller parameters are constructed to self-tune the impedance parameters, so as to optimize the impedance control of the end-effector and achieve compliant picking. Finally, the control system simulation model and the harvesting robot experiment setup are established, respectively. The effectiveness of the proposed method is verified by simulation comparison and grasping experiments carried out on harvesting robot.

2. Materials and Methods

2.1. Viscoelastic Burgers Model of Apple and Parameter Acquisition. Apple is essentially a kind of viscoelastic body with rheological characteristics. When it is loaded, it will produce flow and deformation and internal structural characteristics of the fruit had an obvious effect on the mechanical damage behavior of the tissues [10]. Applying the viscoelastic model to describe the rheological characteristics of apple can better analyze the flow and deformation characteristics of apple under load. Burgers model can represent complex rheological properties such as permanent plastic deformation, instantaneous elastic deformation, and delayed elastic deformation [11]. Therefore, the classical four-element Burgers model is used to characterize the viscoelasticity of apples. The creep constitutive equation of the Burgers model is as follows [12, 13]:

$$\frac{\mathrm{d}^2 f}{\mathrm{d}t^2} + \left(\frac{e_1}{\eta_1} + \frac{e_2}{\eta_2} + \frac{e_1}{\eta_2}\right) \cdot \frac{\mathrm{d}f}{\mathrm{d}t} + \frac{e_1 \cdot e_2}{\eta_1 \cdot \eta_2} f = e_1 \ddot{x} + \frac{e_1 \cdot e_2}{\eta_2} \dot{x}, \tag{1}$$

where f is the contact force between the apple and end-effector finger (N). x is fruit deformation (mm). t is time (s). e_1 is instantaneous elastic modulus ($\mathrm{N \cdot mm^{-1}}$). e_2 is retarded elastic modulus ($\mathrm{N \cdot mm^{-1}}$). η_1 is the viscosity coefficient of series viscous elements ($\mathrm{N \cdot s \cdot mm^{-1}}$). η_2 is the viscosity coefficient of parallel viscous elements ($\mathrm{N \cdot s \cdot mm^{-1}}$).

The uniaxial compression test under constant pressure was carried out on the 10 groups of apple samples by using a TA-XT2i/25 texture analyzer. The loading time of each group was 2000 s. After the completion of each group, the data of fruit deformation were screened and 30 data were selected. Combining equation (1), the Burgers creep model of apple under constant force is expressed as follows:

$$x = \frac{f}{e_1} + \frac{f}{\eta_1} \cdot t + \frac{f}{e_2} \cdot \left(1 - e^{-(e_2/\eta_2) \cdot t}\right). \tag{2}$$

After all creep experiments are completed, the data are averaged. The MATLAB fitting toolbox is used to fit the data by equation (2). The fitting results are shown in Figure 1.

The sum of variance and standard deviation of curve fitting results in Figure 1 are 0.00071 and 0.0052, respectively. The fitting results verify the validity of the selected model. The viscoelastic parameters of apples can be obtained from above. $e_1 = 24.43\ \mathrm{N \cdot mm^{-1}}$, $e_2 = 50.88\ \mathrm{N \cdot mm^{-1}}$, $\eta_1 = 1.27e^6\ \mathrm{N \cdot s \cdot mm^{-1}}$, and $\eta_2 = 2.03e^4\ \mathrm{N \cdot s \cdot mm^{-1}}$.

2.2. Viscoelastic Apple Grasping Model and Analysis of Its Mechanical Properties

2.2.1. Viscoelastic Apple Grasping Model. Because apple is the spherical fruit, the globoid end-effector has better envelope in the grasping process. It can increase the contact area between the fingers of end-effector and the grasped fruit. The globoid end-effector reduces the contact pressure as well. Thus, the end-effector of apple harvesting robot adopts globoid double-fingered configuration [14]. The double finger end-effector of apple harvesting robot is shown in Figure 2. The end-effector is driven by a DC motor with self-locking function. The fingers opening and closing of the end-effector is driven by a constant speed mode. In the process of grasping apple, the fingers contact the apple and continue to close to deform the apple, the end-effector will not slow down, and stop closing until the output force of end-effector reaches the maximum value F_0. Therefore, the grasping process of end-effector includes three stages: the constant loading stage, the overload deceleration stage, and the stress relaxation stage.

At the constant loading stage, the fruit deformation was linearly related to time. The initial conditions are as follows: $\dot{x}_1 = v_0$, $\ddot{x}_1 = 0$.

At the overload deceleration stage, the output force of the end-effector reaches the maximum of F_0. The fruit contact force will continue to increase due to the inertia of the end-effector finger, which is greater than the output grasping force, and the fingers will slow down to stop at this

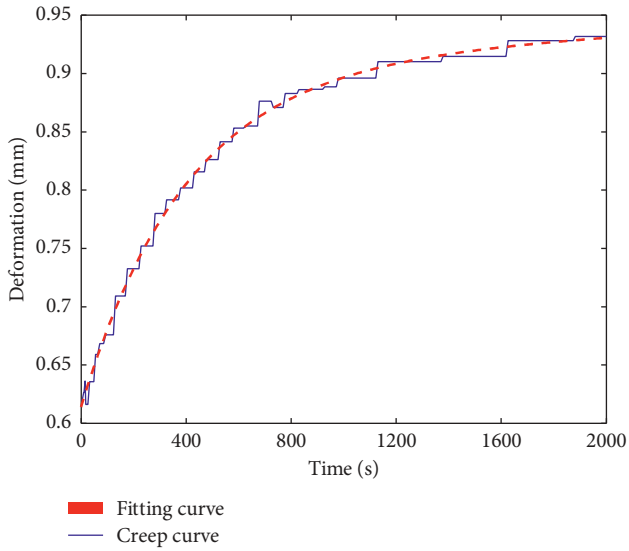

Figure 1: Curve fitting result of creep data.

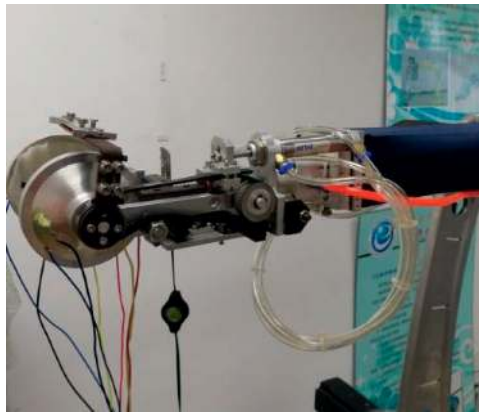

Figure 2: End-effector of apple harvesting robot.

time. The kinematics equation is $m_e\ddot{x}_2 = F_0 - f$, where m_e is the equivalent mass of the end-effector electromechanical system.

At stress relaxation stage, fruit deformation did not change, and the initial condition is $x_3 = 0$.

According to the abovementioned conditions, combining equation (1), three stages of grasping model solutions are obtained as follows in turn:

$$\begin{cases} \dfrac{d^2 f}{dt^2} + \left(\dfrac{e_1}{\eta_1} + \dfrac{e_2}{\eta_2} + \dfrac{e_1}{\eta_2}\right) \cdot \dfrac{df}{dt} + \dfrac{e_1 \cdot e_2}{\eta_1 \cdot \eta_2} f = \dfrac{e_1 \cdot e_2 \cdot v_0}{\eta_2}, \\ \dfrac{d^3 f}{dt^3} + \left(\dfrac{e_1}{\eta_1} + \dfrac{e_2}{\eta_2} + \dfrac{e_1}{\eta_2}\right) \cdot \dfrac{d^2 f}{dt^2} + \left(\dfrac{e_1 \cdot e_2}{\eta_1 \cdot \eta_2} + \dfrac{e_1}{m_e}\right) \\ \cdot \dfrac{df}{dt} + \dfrac{e_1 \cdot e_2}{m_e \cdot \eta_2} \cdot f = \dfrac{e_1 \cdot e_2 \cdot F_0}{m_e \cdot \eta_2}, \\ \dfrac{d^2 f}{dt^2} + \left(\dfrac{e_1}{\eta_1} + \dfrac{e_2}{\eta_2} + \dfrac{e_1}{\eta_2}\right) \cdot \dfrac{df}{dt} + \dfrac{e_1 \cdot e_2}{\eta_1 \cdot \eta_2} f = 0. \end{cases} \tag{3}$$

From the abovementioned equations, it is known that the variations of fruit deformation with time in the stage of constant loading and stress relaxation are $x_1 = kt$ and $x_3 = 0$, respectively, where k is a constant. Next, the equation of fruit deformation during the overload deceleration stage is solved.

According to Deb et al., the discriminant of the characteristic equation of the second equation in formula (3) in the overload deceleration stage is greater than 0. Therefore, by solving the characteristic equation of the second equation, one real root λ_1 and two conjugate complex roots $\alpha \pm \beta i$ can be obtained. The solution of the equation is as follows.

$$f = F_0 - C_1 e^{\lambda_1 T} + e^{\alpha T}\left(C_1 \cos \beta T + C_2 \sin \beta T\right), \tag{4}$$

where $T = t - t_0$, and t_0 is the starting time of overload deceleration. According to the initial value condition $f(t_0) = F_0$, $\dot{x}_2(t_0) = v_0$, and $x_2(t_0) = v_0 \cdot t_0$, it can be obtained that

$$\begin{cases} C_1 = \dfrac{m v_0 \alpha \beta \lambda_1^2 \left(\alpha \beta t_0 - 2\right)}{2\beta\lambda_1^2 + \alpha^2\lambda_1^2 + \alpha^2\beta^2 - \beta^2\lambda_1^2 - 2\alpha\beta\lambda_1}, \\ C_2 = m v_0 \beta + m v_0 \dfrac{\alpha\beta^3\lambda_1^2 t_0 - 2\beta^2\lambda_1^2 - \alpha^2\beta^3\lambda_1 t_0 + 2\alpha\beta^3\lambda_1}{2\beta\lambda_1^2 + \alpha^2\lambda_1^2 + \alpha^2\beta^2 - \beta^2\lambda_1^2 - 2\alpha\beta\lambda_1}, \end{cases} \tag{5}$$

where C_1 and C_2 are constants proportional to v_0. Combining $m_e\ddot{x} = F_0 - f$ with equation (4), the following can be obtained:

$$\ddot{x}_2 = C_1 e^{\lambda_1 T} - e^{\alpha T}\left(C_1 \cos \beta T + C_2 \sin \beta T\right). \tag{6}$$

By integrating equation (6), the equation of fruit deformation with time during the overload deceleration stage can be obtained:

$$\begin{aligned} x_2 = {} & \frac{C_1}{\lambda_1^2} \cdot C_2^{\lambda_1 T} - \frac{\left(\alpha^2 \cdot C_1 - 2 \cdot \alpha \cdot \beta \cdot C_2 - C_1 \cdot \beta^2\right)}{\left(\alpha^2 + \beta^2\right)^2} C_2^{\alpha T} \\ & \cdot \cos(\beta T) \\ & - \frac{\left(e \cdot \alpha^2 + 2 \cdot \alpha \cdot C_1 \cdot \beta - e \cdot \beta^2\right)}{\left(\alpha^2 + \beta^2\right)^2} C_2^{\alpha T} \cdot \sin(\beta T). \end{aligned} \tag{7}$$

2.2.2. Analysis of Mechanical Characteristics of Apple Grasping. According to the three-stage compound dynamic model of the grasping process, we take six different grasping velocities ($v_0 = 0.1\ \text{mm·s}^{-1}$, $v_0 = 0.5\ \text{mm·s}^{-1}$, $v_0 = 1\ \text{mm·s}^{-1}$, $v_0 = 5\ \text{mm·s}^{-1}$, $v_0 = 10\ \text{mm·s}^{-1}$, and $v_0 = 15\ \text{mm·s}^{-1}$) for analysis. On the basis of our previous studies, the law of fruit deformation with time and the law of contact force with time under six grasping velocities were obtained [16]. Thus, the relationship between contact force and deformation of apple grasping in three stages is shown in Figure 3.

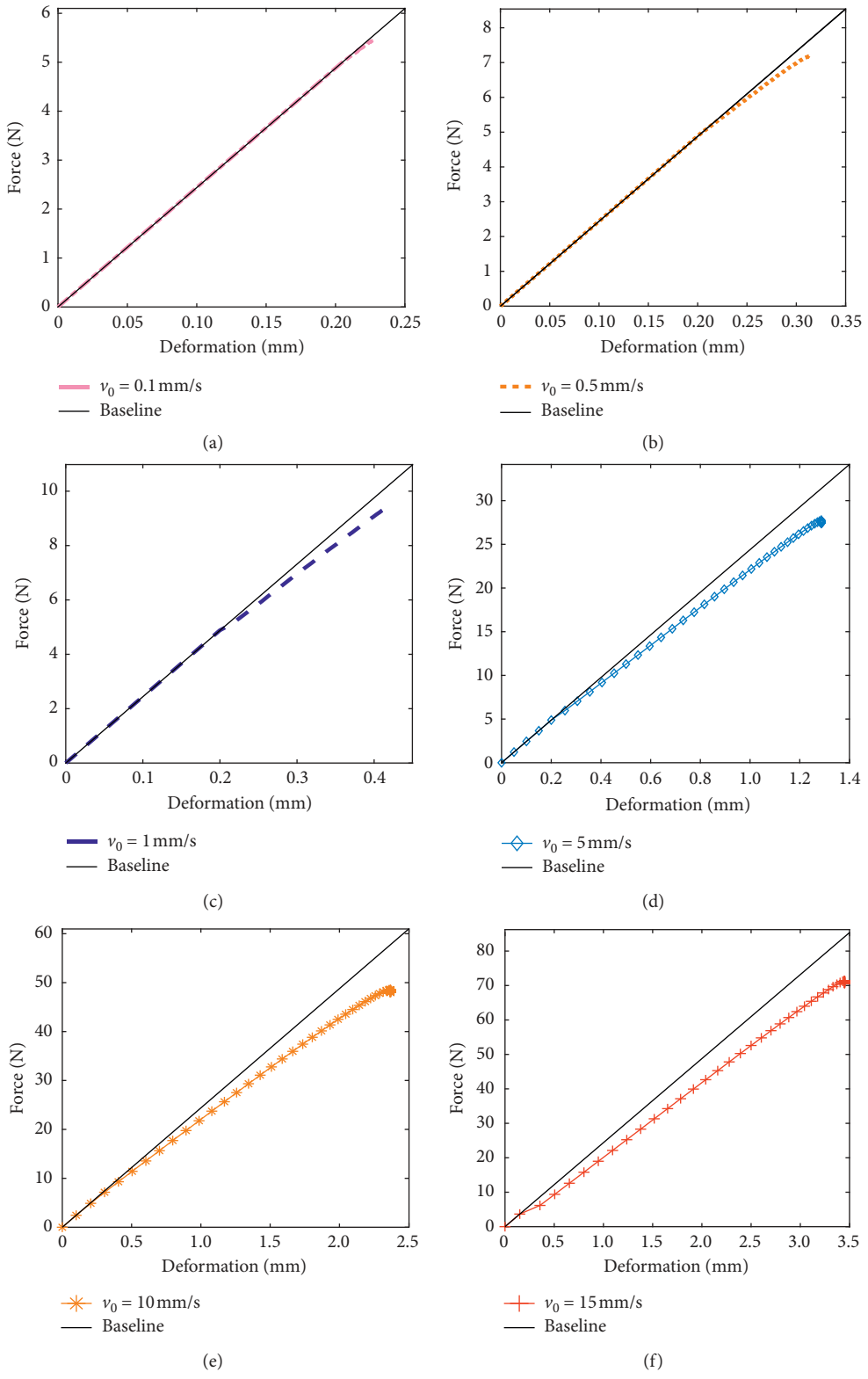

Figure 3: Curves of contact force with fruit deformation at different grasping velocities. (a) $v_0 = 0.1\ \text{mm}\cdot\text{s}^{-1}$. (b) $v_0 = 0.5\ \text{mm}\cdot\text{s}^{-1}$. (c) $v_0 = 1\ \text{mm}\cdot\text{s}^{-1}$. (d) $v_0 = 5\ \text{mm}\cdot\text{s}^{-1}$. (e) $v_0 = 10\ \text{mm}\cdot\text{s}^{-1}$. (f) $v_0 = 15\ \text{mm}\cdot\text{s}^{-1}$.

In the initial constant loading stage of the fruit grasping process, the contact force is approximately proportional to the deformation. The ratio is 24.43 N/mm from the test data of contact force and deformation. In order to facilitate comparative analysis, the baseline with a slope of 24.43 is given, as shown in Figure 3. In the overload deceleration

stage, the relationship curve between contact force and deformation deviates from the baseline and the slope decreases continuously. At the same time, the decreasing trend increases with the increase in grasping speed. In the final stress relaxation stage, the fruit deformation does not change any more and the contact force is slowly reduced to no change due to self-locking of end-effector drive motor.

The stiffness of grasping equivalent environment, which is the slope of the contact force-deformation curve, is obtained by the relationship between the contact force and deformation of fruit [17]. It is calculated by two groups of data (f_j, x_j) and (f_{j+1}, x_{j+1}), as shown in Figure 3. The j value of equivalent stiffness of fruit is $k_{ej} = (f_{j+1} - f_j)/(x_{j+1} - x_j)$. The relationship between the equivalent stiffness of grasping and fruit deformation at different grasping velocities is shown in Figure 4.

From Figure 4, it can be seen that the equivalent stiffness is about 24.43 in the constant loading stage. When the grasping process enters the overload deceleration stage, the equivalent stiffness of the environment decreases greatly in a very short time. Then, it decreases very slowly in a subsequent period of time, when the equivalent stiffness can be approximately considered to remain unchanged. With the deceleration movement of the end-effector fingers, the grasping velocity becomes slower and slower, and the equivalent stiffness decreases again. Before the end-effector is about to stop, the equivalent stiffness suddenly changes and immediately decreases to nearly zero.

In this section, using the established composite dynamic equation of the grasping process, the relationship between fruit contact force and deformation is obtained. Furthermore, the change rules of the equivalent stiffness of grasping environment are analyzed. These lay a foundation for the follow-up study of the compliant grasping control.

2.3. Harvesting Robot Grasping Experiment Setup. The experimental platform of apple harvesting robot is shown in Figure 5. The robot mainly consists of an autonomous vehicle, a manipulator, an end-effector, the sensors, the vision system, and control system. The manipulator with 5 degrees of freedom prismatic-revolute-revolute-revolute-prismatic (PRRRP) structure is geometrically optimized to provide quasilinear behavior and to simplify the control strategy. The end-effector with the DC motor-driven gripper is designed to satisfy the requirements for harvesting apple. The harvesting robot autonomously performed its harvesting task using a vision-based module. The fruit recognition algorithm is developed to detect and locate the apple automatically. The control system, including industrial computer and servo driver, conducts the manipulator and the end-effector as it approaches and picks the apples [18]. Before grasping, the image acquisition system recognizes and processes the image of the target fruit [19, 20], so as to control the end-effector to stretch out to carry out the grasping task. In the process of grasping, the contact force feedback signal between fruit and end-effector fingers is detected by using a FSR-402 force-sensitive resistance sensor. The signal is collected by data acquisition card and sent to an industrial computer. Then, the grasping control task is completed by using an industrial computer. The force calibration method of FSR sensor is to use a set of standard weights to calibrate and a custom filter is designed to deal with data acquisition to improve the accuracy of calibration [21].

2.4. Grasping Control of End-Effector of Harvesting Robot

2.4.1. Modeling of the End-Effector Drive Control System. The transmission mechanism of the grasping system of the harvesting robot end-effector and the model of the driving system composed of reducer and DC motor are shown in Figure 6.

In Figure 6, u_c is the control voltage and n is the reduction ratio of the deceleration device. The motor rotation angle θ_m is transformed into load rotation angle θ_l by a deceleration device. x is the linear movement displacement of the end-effector finger after contacting the fruit. The relationship between the end-effector finger displacement x and the load rotation angle θ_l is $x = c \cdot \theta_l / 2\pi$ and c is the lead of ball screw. The kinematics equation of DC motor is as follows:

$$T_e = J\ddot{\theta}_m + D\dot{\theta}_m + T_c + T_o, \tag{8}$$

where D is the viscous friction coefficient of motor, J is the inertia of motor, T_o is the load torque converted to motor, T_c is the unknown friction moment, and T_e is the electromagnetic torque. According to Kirchhoff's law,

$$L\frac{\mathrm{d}i}{\mathrm{d}t} + Ri + E = u_m, \tag{9}$$

where R is armature resistance and L is inductance. The motor electromagnetic torque equation is

$$T_e = K_t i, \tag{10}$$

where i is armature current and K_t is the motor's torque constant. The back EMF equation is as follows:

$$E = K_b \dot{\theta}_m, \tag{11}$$

where E is the motor back EMF and K_b is the back EMF constant. The power amplifier equation is

$$u_m = K_s u_c, \tag{12}$$

where u_m is the armature voltage of the motor and K_s is power amplification factor. The driving link is

$$\begin{cases} \theta_m = n\theta_l, \\ \\ n = \dfrac{T_l}{T_n}, \end{cases} \tag{13}$$

where T_l is the actual load torque and T_n is the load torque converted to the motor end. In general, the inductance L of DC motor is very small, so let $L = 0$. The general second-order model of the end-effector can be obtained from (8)–(13):

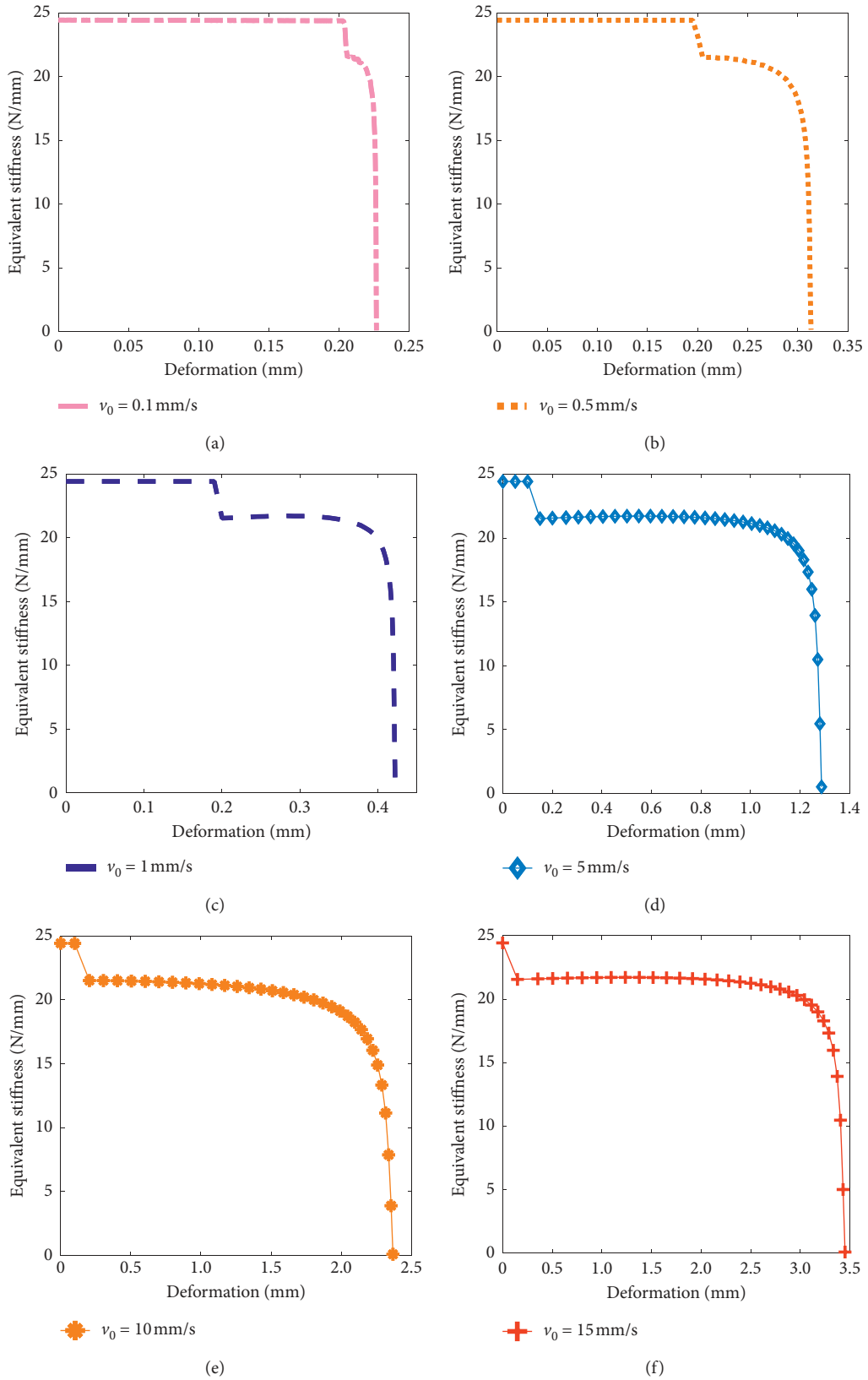

FIGURE 4: Curves of equivalent stiffness of grasping environment with fruit deformation at different grasping velocities. (a) $v_0 = 0.1$ mm·s^{-1}. (b) $v_0 = 0.5$ mm·s^{-1}. (c) $v_0 = 1$ mm·s^{-1}. (d) $v_0 = 5$ mm·s^{-1}. (e) $v_0 = 10$ mm·s^{-1}. (f) $v_0 = 15$ mm·s^{-1}.

Figure 5: The grasping experimental platform for apple harvesting robot.

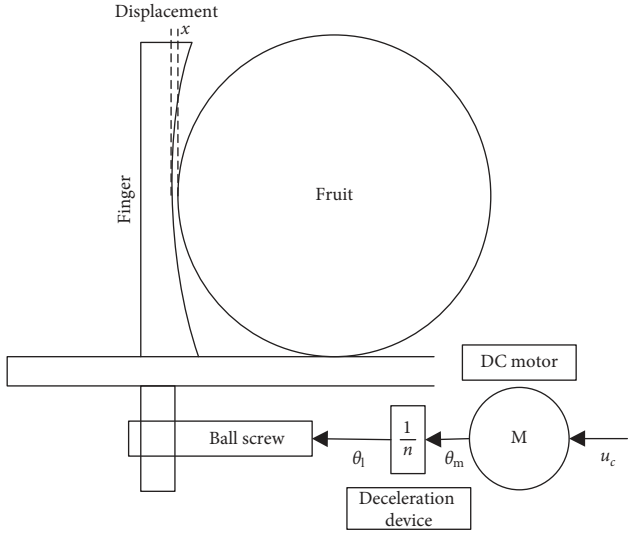

Figure 6: Driving mechanism and the end-effector model.

$$Au_c = \ddot{Q} + B\dot{Q} + \xi_0, \tag{14}$$

where $A = K_t k_s c/nRJ$, $B = (D/J + K_t K_b/RJ)$, and $\zeta_0 = (T_{\text{Coul}} + (T_n/n))/Jn$. A and B are system gain, u_c is system input, Q is actual load torque, and $Q = c\theta_l$. ζ_0 is a constant disturbance because the controller is required to be robust to ζ_0; let $\xi_0 = 0$. The transfer function of equation (14) is obtained by Laplace transformation.

$$G(s) = \frac{Q(s)}{u_c(s)} = \frac{A}{s(s+B)}. \tag{15}$$

According to Ji et al., the motor back EMF constant $K_b = 0.7$, motor torque constant $K_t = 0.9$, motor armature resistance $R = 1.5\,\Omega$, power amplification factor $K_s = 50$, motor inertia $J = 0.1\ \text{kg}\cdot\text{m}^2$, motor viscous friction coefficient $D = 0.38$, gear reduction ratio $n = 50$, and the lead of ball screw is 3.14 mm. Therefore, the mathematical model of the end-effector is as follows:

$$G(s) = \frac{x(s)}{u_c(s)} = \frac{6}{s^2 + 8s}. \tag{16}$$

2.4.2. Grasping Force Impedance Control Strategy. In the grasping process of the end-effector, apple is subjected to the grasping force to produce contact force and deformation. The deformation is equivalent to the forward displacement of the end-effector fingers and acts as the desired position input of the control system. The traditional impedance control can make the force and position achieve a good dynamic relationship [23]. According to the analysis in reference [16], when the grasping velocity is greater than $3\ \text{mm}\cdot\text{s}^{-1}$, the apple skin will undergo plastic deformation. Considering the real-time performance of the robot grasping fruits, the grasping velocity of $3\ \text{mm}\cdot\text{s}^{-1}$ is selected. Through the solution and analysis in Section 2.2.2, the deformation, deformation velocity, and deformation acceleration of apple under grasping, i.e., the desired position, desired velocity, and desired acceleration, are obtained, as shown in Figure 7.

The force/position control system in the grasping process is modeled as an impedance model of the second-order differential equation of mass-damp-spring [24]. The relationship between the end position of end-effector and the contact force is adjusted by tuning the impedance controller parameters. Taking the end-effector of double fingers structure with single degree of freedom as an example, the force-based impedance equation is as follows [25]:

$$m_d(\ddot{x} - \ddot{x}_d) + b_d(\dot{x} - \dot{x}_d) + k_d(x - x_d) = F_r, \tag{17}$$

where m_d, b_d, and k_d are inertia, damping, and stiffness parameters of impedance controller, respectively.

Choosing appropriate impedance parameters can make the end-effector fingers to touch apple quickly and smoothly, which ensures the compliance of clamping apple [26]. According to the impedance relationship of equation (17), the force-based impedance control block diagram is obtained, as shown in Figure 8.

In Figure 8, $\dot{x}_d$ and $\ddot{x}_d$ represent the desired velocity and acceleration of end-effector ($\text{mm}\cdot\text{s}^{-1}$ and $\text{mm}\cdot\text{s}^{-2}$). $\dot{x}$ and $\ddot{x}$ represent the actual velocity and acceleration of end-effector ($\text{mm}\cdot\text{s}^{-1}$ and $\text{mm}\cdot\text{s}^{-2}$). x_e is the environmental location (mm). The outer loop inputs the actual trajectory and the desired trajectory of the end-effector into the impedance model to obtain the desired force. The inner loop takes the error between the desired force and the actual contact force as the input. The input is adjusted by PID. Finally, according to the mathematical model of the end-effector, the output of the actual position is obtained.

As shown in Figure 9, the grasping environment is a new second-order system formed when the end-effector fingers contact with the apple. It includes the impedance characteristics of both the fruit and the end-effector systems. In Figure 9, m_e, b_e, and k_e represent the inertia, damping, and stiffness parameters of the environmental model, respectively.

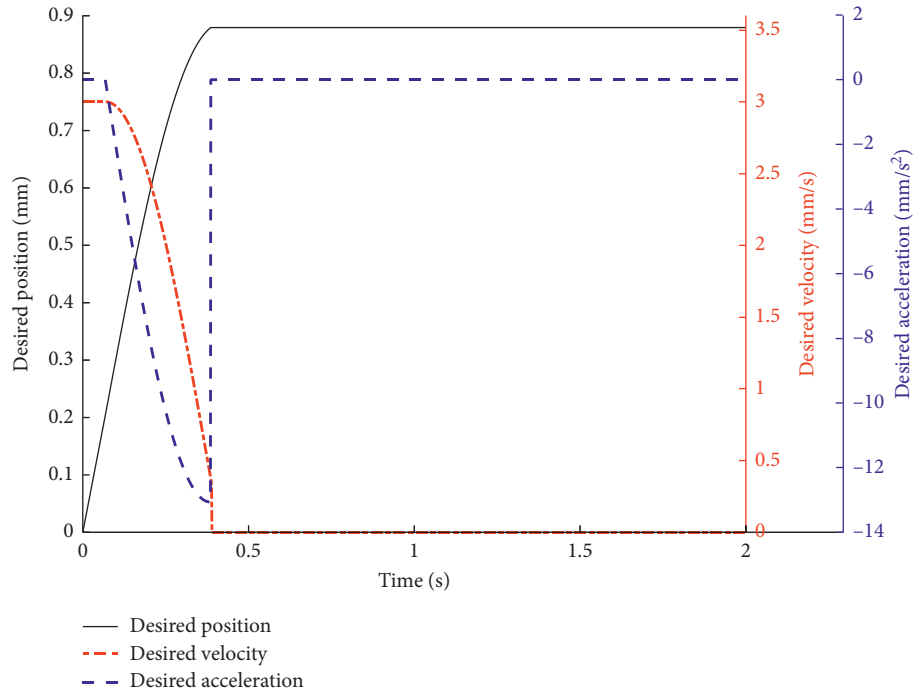

Figure 7: Desired position, velocity, and acceleration curves of the impedance control system.

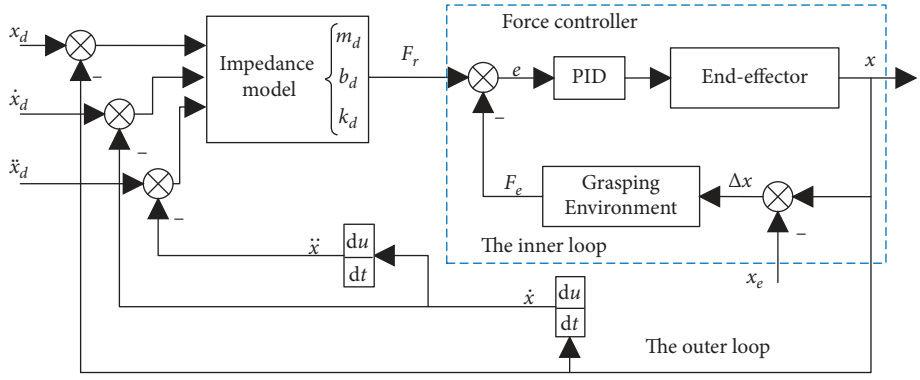

Figure 8: Diagram of the force-based impedance control system.

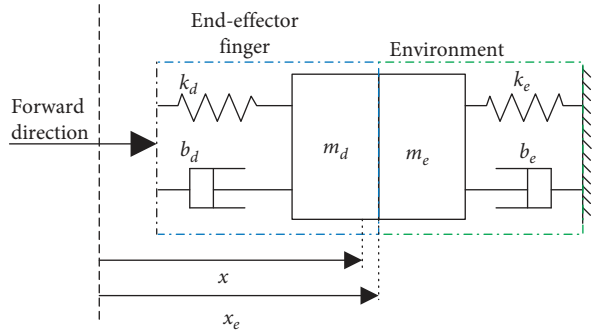

Figure 9: Model of grasping environment.

When the end-effector fingers touch the apple, the apple will be deformed by extrusion. According to the principle of impedance, the deformation of apple will produce contact force F_e. Let $\triangle x = x - x_e$ because the change rate of $\triangle x$ is very small and usually takes $m_e \triangle \ddot{x} \approx 0$, $b_e \triangle \dot{x} \approx 0$. The grasping environment contact force model caused by fruit deformation is equivalent to a first-order model [27].

$$F_e = k_e (x - x_e) = k_e \triangle x, \tag{18}$$

where k_e is the stiffness of fruit (N/mm).

However, as can be seen from the analysis in the preceding section, because of the larger equivalent stiffness of grasping environment, the smaller position error will lead to great contact force deviation. Besides, the environmental stiffness and location parameter are also uncertain [28]. Due to the different grasping objects, there is no systematic method to measure the environmental parameters. For reducing the influence of environmental parameter uncertainties on the impedance controller performance of end-

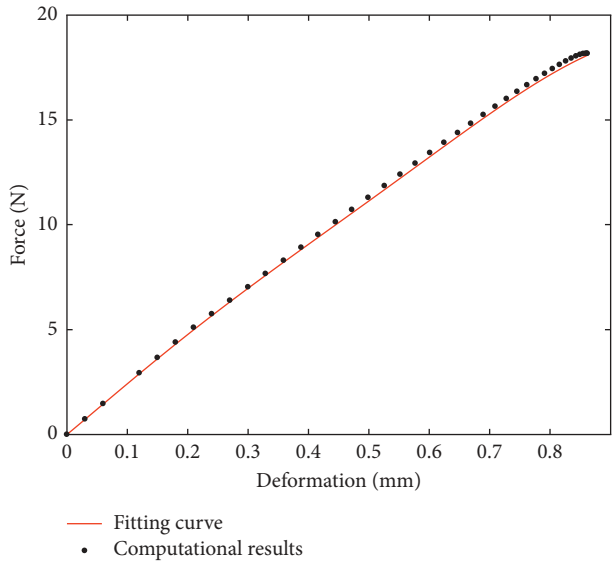

FIGURE 10: Fitting curve of the grasping environment contact force model.

effector, the grasping environment contact force model is fitted by using MATLAB at the speed of 3 mm·s^{-1} according to the abovementioned law of fruit force and deformation. The fitting result is shown in Figure 10.

The equation of the grasping environment contact force model fitting is obtained as follows:

$$F_e = 7.181 - 9.035\cos(2.756x) + 7.268\sin(2.756x) + 1.853\cos(5.512x) + 0.7199\sin(5.512x). \quad (19)$$

The variance and standard deviation of fitting results are 0.03576 and 0.03152, respectively.

2.4.3. Self-Tuning of Impedance Control Parameters. According to the impedance control diagram shown in Figure 8 and the overall mathematical model of the end-effector, the control performance is tested by taking into account the overshoot, response speed, adjustment time, and steady-state error. The parameters of the impedance controller are set as fixed values at first. According to the principle of determining and adjusting impedance parameters m_d, b_d, and k_d [29], taking the grasping control of apple harvesting robot in our laboratory as an example, the fixed impedance parameters are set as follows: the inertia parameter $m_d = 0.05$ N·s·mm^{-2}, damping parameter $b_d = 1.5$ N·s·mm^{-1}, and stiffness parameter $k_d = 15$ N·mm^{-1}. The environmental location is 5 mm. The parameters of PID controller, which are determined by the trial and error method, are proportional parameter $K_p = 2.68$ and integral parameter $K_i = 5.03$. Because the introduction of differential parameters may reduce the control system accuracy in the case of disturbance, take $K_d = 0$. By substituting the fixed parameters into the system, the compliant grasping control of fruits can be achieved by combining the grasping environment and the mathematical model of the end-effector.

However, due to the unknown and uncertain complex environment information, the fixed parameters impedance controller does not have good adjustment ability [30]. Therefore, it is necessary to study the method of impedance parameters self-tuning. The influence of different impedance control parameters on the output force will be analyzed in following sections. The variation functions of inertia, damping, and stiffness parameters are constructed so that the contact force can track the desired force more quickly and effectively.

(1) Design of the Inertia Parameter m_d Self-Tuning Function. Fix the damping and stiffness parameters of the impedance controller; let $b_d = 1.5$, $k_d = 15$, and m_d equals 0.005, 0.05, and 0.15, respectively. The contact force curves of the force-based impedance control system with different inertia parameters m_d are shown in Figure 11. As shown in Figure 11, with the increase of inertia parameter m_d from 0.005 to 0.15, the response speed of contact force increases and the time reached the peak value becomes less and less. When the inertia parameters become larger, the overshoot of contact force increases. Meanwhile, too large inertia parameters cause the output contact force to oscillate, while too small inertia parameters increase the peak time. Thus, when adjusting the inertia parameter of impedance controller, the desired inertia parameter should be selected without causing the oscillation of the contact force, and it should make the contact force have faster response speed and smaller overshoot.

According to the abovementioned analysis, the designed nonlinear function of the inertial parameter is as follows:

$$m_d(t) = a_m - b_m(1 - \sec h(c_m t)), \quad (20)$$

where t is the simulation time, a_m, b_m, and c_m are the coefficients of the inertial parameter nonlinear function. When $t = 0$, the inertia parameter takes maximum a_m. When t tends to infinity, the inertia parameter takes minimum $a_m - b_m$. c_m is used to adjust the change rate of inertia parameter. $\sec h(x) = 2/(e^x + e^{-x})$ is a hyperbolic secant function. Inertia parameter is large at first, and the response speed is fast. With the grasping process, the inertia parameter is quickly stabilized to the smaller value, which makes the overshoot of contact force as small as possible.

(2) Design of the Damping Parameter b_d Self-Tuning Function. Fix the inertia and stiffness parameters of the impedance controller and analyze the influence of the change of damping parameter on the output contact force f_e. Let $m_d = 0.05$, $k_d = 15$, and b_d equals 0.25, 1.5, and 3.5, respectively. The contact force output of the force-based impedance control system with different damping parameters b_d is shown in Figure 12. According to Figure 12, when the inertia and stiffness parameters are fixed, too small damping parameter will cause the oscillation of contact force and the adjusting time will increase. However, the contact force can still track the desired force eventually. When the value of damping parameter increases, the overshoot of contact force decreases and the response speed decreases. It can be seen that the value of b_d should not only ensure the avoidance of

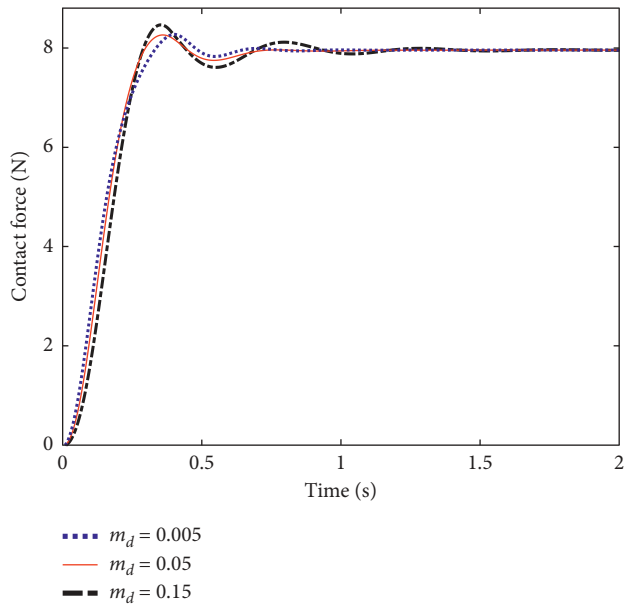

Figure 11: Contact force curves with different inertia parameters.

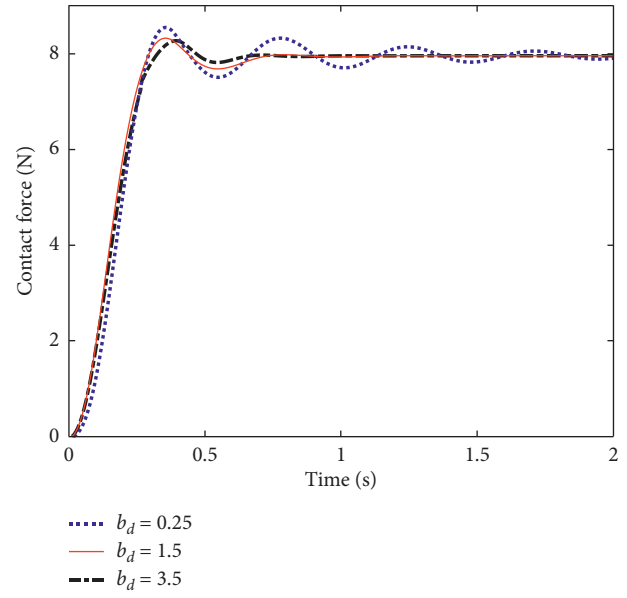

Figure 12: Contact force curves with different damping parameters.

contact force oscillation but also enable the system to have a smaller overshoot and faster response speed.

Based on the abovementioned analysis, the nonlinear function of the damping parameter is designed as follow:

$$b_d(t) = a_b + b_b(1 - \sec h(c_b t)), \tag{21}$$

where a_b, b_b, and c_b are the coefficients of the damping parameter nonlinear function. When $t = 0$, the minimum value of the damping parameter is a_b. When t tends to infinity, the maximum value of the damping parameter is $a_b + b_b$. c_b is used to adjust the change rate of damping parameters. The initial value of damping parameter is selected to make the initial response speed faster and avoid oscillation. Then, the damping parameter is reduced to obtain better reverse regulation performance.

(3) Design of the Stiffness Parameter k_d Self-Tuning Function. Fix the inertia and damping parameters of the impedance controller, and analyze the influence of stiffness parameter on the output contact force. Let $m_d = 0.05$, $b_d = 1.5$, and k_d equals 3, 15, and 30, respectively. The contact force output of the force-based impedance control system with different stiffness parameters m_d is shown in Figure 13. According to Figure 13, the final stability values of contact force are different under different stiffness parameters. The greater the stiffness parameter, the greater the contact force stability. It shows that the stiffness parameter determines the desired output force of outer loop impedance controller in control system. When the stiffness parameter is small, the final contact force is about 2.34 N, the overshoot is about 74%, and the peak time is about 0.27 s. When the stiffness parameter is large, the contact force is stable at 11.22 N. The contact force reached its peak at 0.42 s is about 11.21 N. It can be seen that with the increase of stiffness parameter, the contact force and the peak time all increase, but the response speed is fast and the overshoot decreases significantly.

According to the abovementioned analysis, the stiffness parameter should guarantee the response speed of contact force at the beginning. Then, it reduces to keep the contact force at the final stable value. Consequently, the designed nonlinear function of the stiffness parameter is as follows:

$$k_d(t) = a_k - b_k(1 - \sec h(c_k t)), \tag{22}$$

where a_k, b_k, and c_k are the coefficients of the stiffness parameter nonlinear function.

Substituting equations (20)–(22) into equation (17), we get a new impedance control equation, $m_d(t)\ddot{E} + b_d(t)\dot{E} + k_d(t)E = F_r$, where $E = x - x_d$. The second-order transfer function of the impedance model is obtained by Laplace transform:

$$K(s) = \frac{F_r(s)}{E(s)} = \frac{1}{m_d s^2 + b_d s + k_d}. \tag{23}$$

The improved impedance control model is simulated below.

3. Results and Discussion

3.1. Analysis of Force-Based Impedance Control Simulation Results. To verify the effectiveness and rapidity of force-based impedance control in tracking desired grasping force, a simulation model of the apple grasping control system with uniform end-effector speed, as shown in Figure 14, is built in SIMULINK. In Figure 14, the grasping environment contact force model is a function represented by equation (19). The force controller is composed of the PID algorithm and the end-effector transfer function.

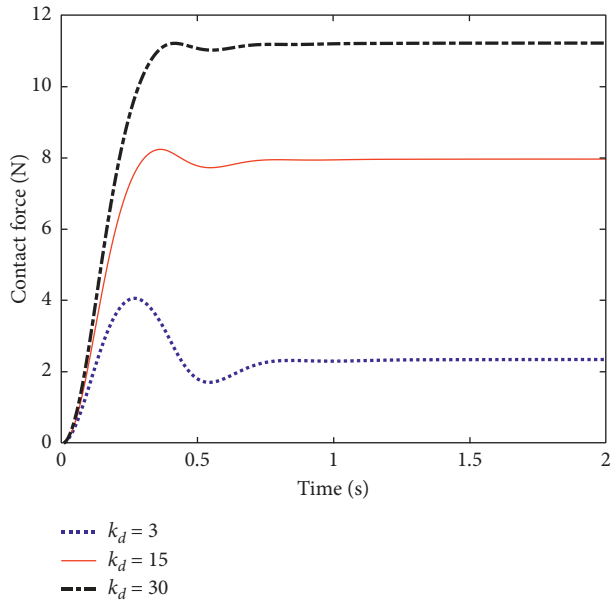

Figure 13: Contact force curves with different stiffness parameters.

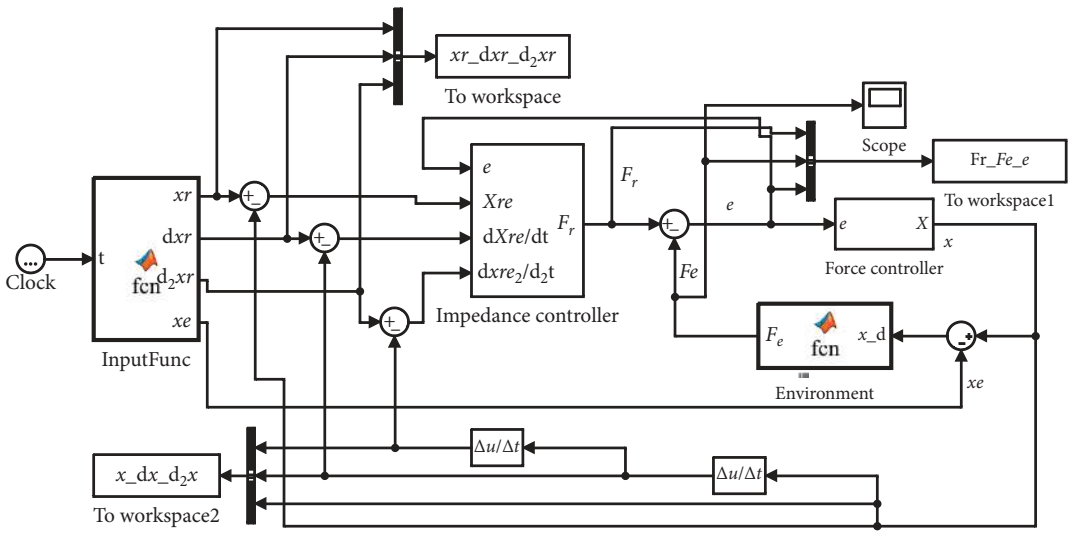

Figure 14: Simulation model of force-based impedance control.

3.1.1. Traditional Impedance Control with Fixed Parameters. The simulation results of the grasping force impedance control with fixed parameters given in Section 2.4.3 are shown in Figure 15.

From Figure 15(a), it can be seen that the desired force calculated by the impedance controller according to the desired position, velocity, and acceleration fluctuates greatly in the initial stage. After that, the change of desired force is relatively smooth. It is a peak at 0.42 s, which is about 8.21 N, and finally stabilize at 7.97 N. Under the force controller, the contact force reaches its peak value at 0.36 s and the overshoot is about 3.2%. Then, it converges rapidly and tends to be stable. Here, the force error is equal to 0. It shows that the designed impedance controller has good real-time performance and no jitter. The force controller enables the contact force to track the desired force quickly and low overshoot.

Figure 15(b) shows that the maximum actual position of end-effector finger is 0.36 mm. Its rate of change reaches zero for the first time. Then, the final stability value of the actual position is 0.35 mm. Through the two curves of actual position change rate and actual position change acceleration, the change of actual position in the simulation process can be observed more clearly. In the initial stage, the actual position changes rapidly and reaches the maximum speed of 1.77 mm·s^{-1} at 0.13 s. The end-effector finger's forward acceleration is 0 mm·s^{-2}. Then, the finger begins to decelerate, and the increase in the amount of finger position begins to slow down until it reaches a maximum. Due to the overshoot of contact force, the controller adjusts backward. When the actual position change rate reaches zero again, the actual position reaches the first trough. The value is about 0.33 mm. After an

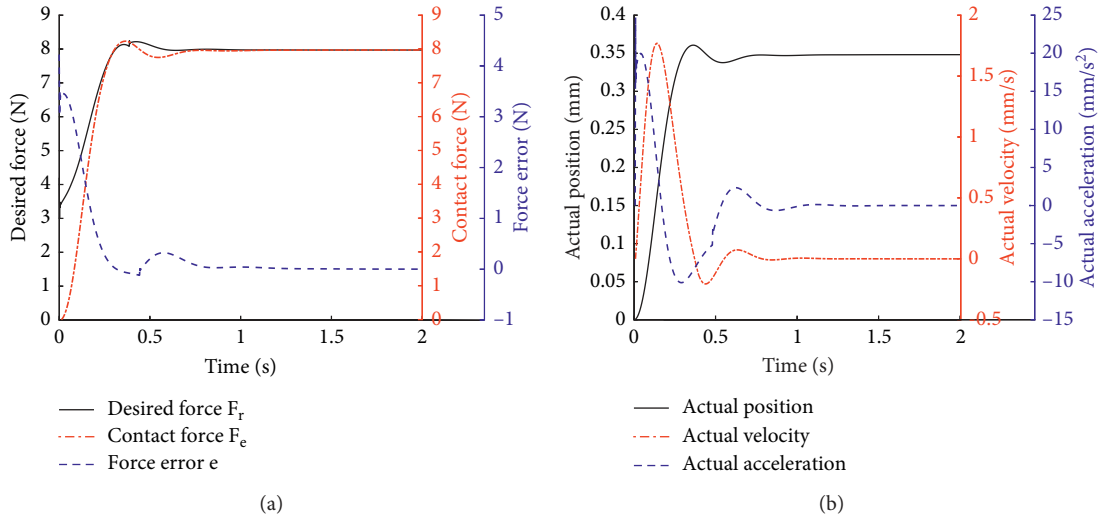

FIGURE 15: Simulation results of grasping force control with fixed parameter impedance control. (a) Curves of desired force, contact force, and force error varying with time. (b) Curves of actual position, velocity, and acceleration varying with time.

acceleration and deceleration movement, the actual position of the end-effector finger is stable and the grasping process is completed.

3.1.2. Improved Impedance Control with Self-Tuning Parameters. Simulation is performed using the model in Figure 14 according to equations (20)–(22). According to the analysis of the influence of impedance parameters on contact force and the properties of hyperbolic sec $h(x)$ in Section 2.4.3, the designed nonlinear function ensures that the contact force has a faster initial response speed and a smaller overshoot and can avoid oscillation, so as to achieve stability. Then, the coefficients a_m and a_k are larger, and a_b is smaller, i.e., $a_m = 0.05$, $a_b = 1.5$, and $a_k = 20$. The coefficients $b_m = 0.04$, $b_b = 0.2$, and $b_k = 15$. To ensure that the parameters of the nonlinear functions have a faster change rate, the coefficients $c_m = 20$, $c_b = 20$, and $c_k = 20$. The simulation results based on improved impedance control are shown in Figure 16.

As shown in Figure 16(a), the desired force of improved impedance control is smoother and the overshoot is about 2.3%. Meanwhile, the peak time is smaller, and the response speed is faster than the traditional impedance control. However, there is a sudden change at 0.4 s. The peak value of the desired force is about 8.3 N, which is larger than that of traditional impedance control. The desired force finally stabilizes at 7.97 N. There is a peak value of contact force at 0.36 s and the overshoot is 2%. Then, the contact force converges rapidly and tends to be stable. At this time, the force error is equal to 0.

Figure 16(b) is a comparison curve of contact force and force error under two impedance control methods. Compared with the traditional impedance controller, the improved impedance controller can make the contact force curve smoother and reduces overshoot by 37.5% under the same conditions. The error fluctuation of contact force and desired force is smaller. The adjustment time of contact force is shorter, which is reduced to 0.48 s. Its compliant control performance is superior to that of traditional impedance control. Under the action of the inner-loop force controller, the contact force can still achieve smooth tracking for desired force even if there is the sudden change of desired force.

The improved impedance control method is proposed for the contact force control in this paper. First, the system input, which is the desired position, is obtained according to the change of fruit deformation with time. Second, aiming at the shortcomings of the traditional first-order model of grasping environment, the grasping environment contact force model is re-established. Finally, aiming at the problem of traditional fixed impedance parameters, the nonlinear function of self-tuning impedance parameters is designed to guarantee that the control system can be better adjusted.

3.2. Analysis of End-Effector Grasping Experiment Results. To verify the performance of the proposed method, the closed-loop grasping experiments are carried out using the traditional impedance control and the improved impedance control, respectively. The grasping experimental platform for harvesting robot is shown in Figure 5. The curves of contact force varying with time during grasping process are obtained, as shown in Figure 17. It can be seen that the end-effector is initially in free space, the time at which the end-effector does not touch the apple and the contact force is 0. When contact occurs, the end-effector moves into the constrained space. At this moment, the designed impedance control algorithm starts to work and adjust the output torque of motor. So, the contact force can track the desired force quickly. When the contact force is stable, the host computer will send the signal of cutting fruit stalk and then issues command to make manipulator move to the designated position. Finally, the motor is driven to reverse and the end-effector releases the apple.

By comparing the experimental curves of the two control methods in Figure 17, it can be found that the contact force curves of the traditional impedance control and the

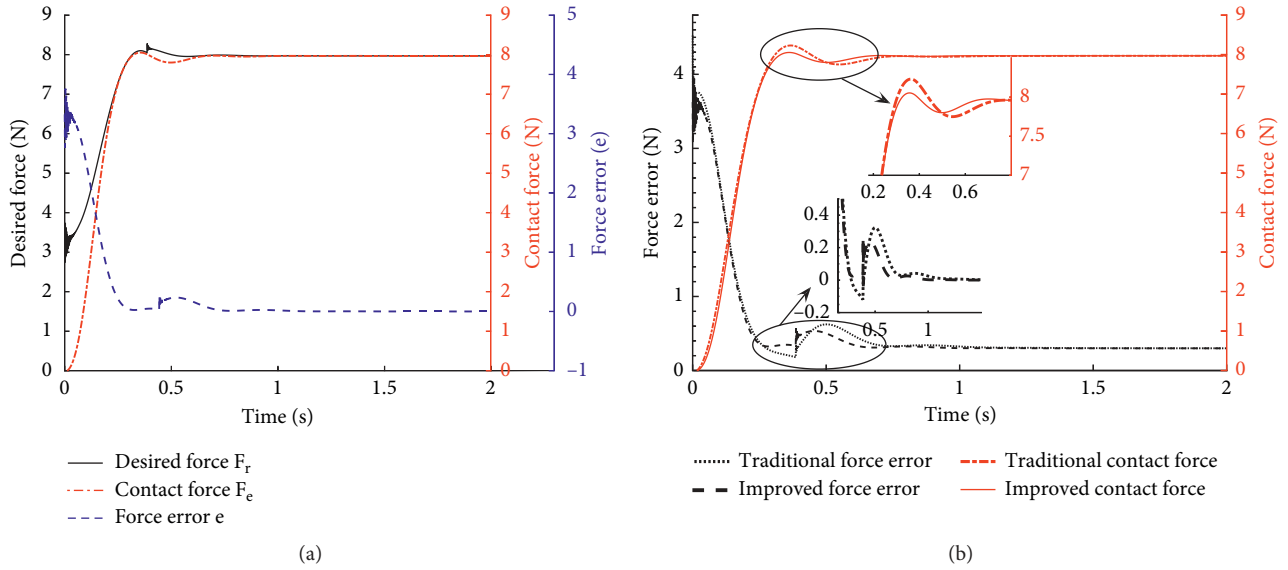

Figure 16: Simulation results of improved impedance control. (a) Curves of desired force, contact force, and force error varying with time. (b) Contact force comparison under two impedance control methods.

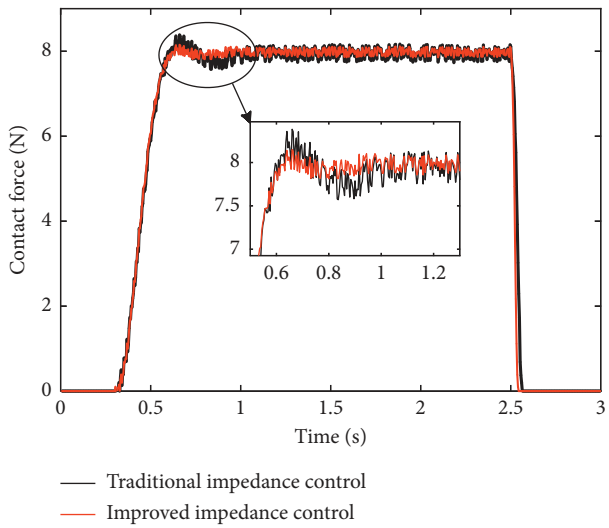

Figure 17: Actual contact force varying with time.

improved impedance control almost reach the peak at 0.64 s, and they are 8.384 N and 8.140 N, respectively. Also, the adjustment time of contact force is basically the same. However, the overshoot of traditional impedance controller is about 3.7%. The overshoot of improved impedance controller is about 1.7%, and the contact force overshoot is significantly reduced. Meanwhile, the contact force of traditional impedance control fluctuates between 7.744 and 8.141 N. While the contact force curve of improved impedance control fluctuates less, between 7.872 and 8.084 N. The improved impedance control fluctuate is about 46% less than that of the traditional one. The contact force changes more smoothly and stably. The improved impedance controller is more suitable for grasping control of picking robot.

When the contact force data of the closed-loop grasping test are collected, there is a slight deviation between the final stability value of each contact force curve and the simulation result of MATLAB. In order to analyze the stability performance of two impedance controllers mentioned above and ensure the stability of the harvesting robot, ten times grasping experiments are carried out on the same apple using two control methods. Set the force measured before release as stable contact force, and the contact force data of grasp test with traditional impedance control method is shown in Table 1.

Similarly, the improved impedance control method is used to carry out the grasp test, and the corresponding contact force data is shown in Table 2.

By analyzing the data in tables 1 and 2, it can be found that the deviation between the contact force obtained by the improved impedance control and the desired force obtained by the simulation is small. The maximum deviation is 9.4%, the minimum deviation is 3.3%, and the average deviation value is 0.465 N. The maximum and minimum deviations of contact force and desired force measured by traditional impedance control are 11% and 6.2%, and the average deviation value is 0.637 N. The average deviation is 27% larger than the one measured by improved impedance control.

3.3. Discussion. According to the results of the above-mentioned simulation and experiment, the author's original intention of this research is further verified. The compliant grasping control of the harvesting robot is realized. Regarding the simulation results of Figure 16(a), by self-tuning of the impedance control parameters, the contact force can quickly respond and track the desired force. It finally reaches a stable value. This shows that the improved impedance control and the desired input obtained by fruit mechanical characteristics both have an effect in the grasping process. The effect is more apparent in the comparison of improved impedance control and traditional impedance control in

Table 1: Contact force data in traditional impedance control.

Number	1	2	3	4	5	6	7	8	9	10
Contact force (N)	7.28	7.45	7.48	7.24	7.09	7.39	7.45	7.28	7.27	7.40
Relative error (%)	8.6	6.5	6.2	9.1	11.0	7.3	6.5	8.6	8.8	7.1

Table 2: Contact force data in improved impedance control.

Number	1	2	3	4	5	6	7	8	9	10
Contact force (N)	7.41	7.65	7.22	7.45	7.68	7.55	7.71	7.39	7.51	7.48
Relative error (%)	7.0	4.0	9.4	6.5	3.6	5.3	3.3	7.0	5.8	6.1

Figure 16(b). The improved contact force overshoot is reduced by 37.5% compared with the traditional one, and the force tracking error is much smaller. It greatly improves the disadvantages of traditional impedance control.

Based on the simulation results, a fruit grasp test was carried out. According to Figure 17, it can be seen that the improved impedance control has a significant effect on the improvement of contact force. Its overshoot has been reduced by approximately 53% compared to the traditional impedance control. The improved contact force fluctuation is smaller, and it is also reduced by about 46% compared with the previous one. Through the comparison between Tables 1 and 2, it can also be found that under the improved impedance control, the force average deviation is smaller.

The results show that after the self-tuning parameters impedance control is applied to the picking robot, the online adjustment ability of the object is effectively improved and the contact force is well controlled. This means that the fruit can be better protected from damage when being grasped. The improved impedance control method, which has better stability and better compliance control performance, is more suitable for grasping control of picking robot. The research results can provide a reference for the compliance control method of apple harvesting robot.

4. Conclusions

The four-element Burgers model is used to describe the rheological characteristics of apples and the relationship between contact force, and time is established at each stage of the grasping process. Combining viscoelastic parameters and initial grasping speed, the relationship between fruit contact force and deformation and the equivalent stiffness of grasping environment during grasping operation are obtained, respectively. The force-based impedance control system is designed. The desired position, velocity, and acceleration are obtained according to the law of fruit mechanical properties. The grasping environment contact force model is established to avoid the errors caused by the first-order environment model. Aiming at the influence of inertia, damping, and stiffness parameters of impedance controller on system overshoot and response time, three time-varying functions of parameters are constructed. Then, an improved impedance control system is obtained.

The effects of fixed parameter traditional impedance control and self-tuning parameters improved impedance control are compared by simulation analysis. The contact force overshoot obtained by traditional impedance control is about 3.2%. Then, it can converge quickly and tend to be stable and the force error will fluctuate greatly at the beginning, which equals 0 with the stability of the contact force. The contact force of improved impedance control has shorter adjusting time and smaller overshoot, which is about 2% and 37.5% less. The fluctuation of force error is obviously reduced. The experimental results also show that the actual contact force overshoot obtained by the improved impedance control is about 1.7%. The average deviation of contact force is 0.465 N, which is 27% less than the traditional impedance control, and the fluctuation of force error is 46% less. The performance of improved impedance control for robot compliant picking is greatly enhanced compared with the traditional impedance control.

Data Availability

The data used to support the findings of this study are available from the corresponding author upon request.

Conflicts of Interest

The authors declare that they have no conflicts of interest.

Acknowledgments

This work was supported by the National Natural Science Foundation of China (NSFC) (grant nos. 61703186 and 61973141) and a project funded by the Priority Academic Program Development of Jiangsu Higher Education Institutions (PAPD-2018-87).

References

[1] W. Ji, G. Chen, B. Xu, X. Meng, and D. Zhao, "Recognition method of green pepper in greenhouse based on least-squares support vector machine optimized by the improved particle swarm optimization," *IEEE Access*, vol. 7, pp. 119742–119754, 2019.

[2] L. Roveda, N. Iannacci, F. Vicentini, N. Pedrocchi, F. Braghin, and L. M. Tosatti, "Optimal impedance force-tracking control design with impact formulation for interaction tasks," *IEEE Robotics and Automation Letters*, vol. 1, no. 1, pp. 130–136, 2016.

[3] Q. Xu, "Robust impedance control of a compliant microgripper for high-speed position/force regulation," *IEEE*

Transactions on Industrial Electronics, vol. 62, no. 2, pp. 1201–1209, 2015.

[4] X. Wang, Y. Xiao, S. Bi, X. Fan, and H. Rao, "Design of test platform for robot flexible grasping and grasping force tracking impedance control," *Transactions of the Chinese Society of Agricultural Engineering*, vol. 31, no. 1, pp. 58–63, 2015.

[5] T. Zhang, L. Jiang, and H. Liu, "A grasping force control strategy for anthropomorphic prosthetic hand," *Robot*, vol. 34, no. 2, pp. 190–196, 2012.

[6] M. Stachowsky, T. Hummel, M. Moussa, and H. A. Abdullah, "A slip detection and correction strategy for precision robot grasping," *IEEE/ASME Transactions on Mechatronics*, vol. 21, no. 5, pp. 2214–2226, 2016.

[7] X. Chen, Z. Li, Y. Wang, and J. Liu, "Effect of fruit and hand characteristics on thumb-index finger power-grasp stability during manual fruit sorting," *Computers and Electronics in Agriculture*, vol. 157, pp. 479–487, 2019.

[8] K. Ba, B. Yu, Z. Gao, Q. Zhu, G. Ma, and X. Kong, "An improved force-based impedance control method for the HDU of legged robots," *ISA Transactions*, vol. 84, pp. 187–205, 2019.

[9] C. Semini, V. Barasuol, T. Boaventura et al., "Towards versatile legged robots through active impedance control," *The International Journal of Robotics Research*, vol. 34, no. 7, pp. 1003–1020, 2015.

[10] Z. Li, P. Li, H. Yang, and J. Liu, "Internal mechanical damage prediction in tomato compression using multiscale finite element models," *Journal of Food Engineering*, vol. 116, no. 3, pp. 639–647, 2013.

[11] B. Zhang, J. Zhou, Y. Meng et al., "Comparative study of mechanical damage caused by a two-finger tomato gripper with different robotic grasping patterns for harvesting robots," *Biosystems Engineering*, vol. 171, pp. 245–257, 2018.

[12] D. Veringa, T. CaSaNdroiu, and G. C. Stan, "Burgers model testing to rheological behavior of apples for strain compression," in *Proceedings of the International Symposium on Agricultural Engineering*, Zurich, Switzerland, 2014.

[13] J. Z. Liu, P. P. Li, and H. P. Mao, "Mechanical and kinematic modeling of assistant vacuum sucking and pulling operation of tomato fruits in robotic harvesting," *Transactions of the ASABE*, vol. 58, no. 3, pp. 539–550, 2015.

[14] W. Ji, Z. Qian, B. Xu, W. Tang, J. Li, and D. Zhao, "Grasping damage analysis of apple by end-effector in harvesting robot," *Journal of Food Process Engineering*, vol. 40, no. 6, Article ID e12589, 2017.

[15] A. Deb, A. Ganguly, G. Sarkar, and A. Biswas, "Numerical solution of third order linear differential equations using generalized one-shot operational matrices in orthogonal hybrid function domain," *Applied Mathematics and Computation*, vol. 219, no. 4, pp. 1485–1514, 2012.

[16] W. Ji, Z. Qian, B. Xu, G. Chen, and D. Zhao, "Apple viscoelastic complex model for bruise damage analysis in constant velocity grasping by gripper," *Computers and Electronics in Agriculture*, vol. 162, pp. 907–920, 2019.

[17] L. Fu and J. Zhao, "Design and implementation of plastic deformation behavior by cartesian impedance control based on maxwell model," *Complexity*, vol. 2018, Article ID 6752752, 9 pages, 2018.

[18] D.-A. Zhao, J. Lv, W. Ji, Y. Zhang, and Y. Chen, "Design and control of an apple harvesting robot," *Biosystems Engineering*, vol. 110, no. 2, pp. 112–122, 2011.

[19] W. Ji, Z. Qian, B. Xu, and D. Zhao, "A nighttime image enhancement method based on retinex and guided filter for object recognition of apple harvesting robot," *International Journal of Advanced Robotic Systems*, vol. 15, no. 1, pp. 1–9, 2018.

[20] W. Ji, X. Meng, Z. Qian, B. Xu, and D. Zhao, "Branch localization method based on the skeleton feature extraction and stereo matching for apple harvesting robot," *International Journal of Advanced Robotic Systems*, vol. 14, no. 3, pp. 1–9, 2017.

[21] X. Wang, Y. Xiao, X. Fan, and Y. Zhao, "Design and grip force control of dual-motor drive electric gripper with parallel fingers," in *Proceedings of the IEEE Information Technology, Networking, Electronic and Automation Control Conference (ITNEC)*, Chongqing, China, May 2016.

[22] W. Ji, D. Luo, J. Li, J. Yang, and D. Zhao, "Compliant grasping force control of end end-effector of fruit and vegetable harvesting robot," *Transactions of the Chinese Society of Agricultural Engineering*, vol. 30, no. 9, pp. 19–26, 2014.

[23] N. Hogan, "Impedance control: an approach to manipulation: Part I-theory," *Journal of Dynamic Systems, Measurement, and Control*, vol. 107, no. 1, pp. 1–7, 1985.

[24] J. Peng, Z. Yang, and T. Ma, "Position/force tracking impedance control for robotic systems with uncertainties based on adaptive jacobian and neural network," *Complexity*, vol. 2019, Article ID 1406534, 16 pages, 2019.

[25] S. Jung, T. C. Hsia, and R. G. Bonitz, "Force tracking impedance control of robot manipulators under unknown environment," *IEEE Transactions on Control Systems Technology*, vol. 12, no. 3, pp. 474–483, 2004.

[26] J. Lee, P. H. Chang, and R. S. Jamisola, "Relative impedance control for dual-arm robots performing asymmetric bimanual tasks," *IEEE Transactions on Industrial Electronics*, vol. 61, no. 7, pp. 3786–3796, 2014.

[27] B. Komati, C. Cédric, and P. Lutz, "Force tracking impedance control with unknown environment at the microscale," in *Proceedings of the IEEE International Conference on Robotics & Automation*, Hong Kong, China, 2014.

[28] H. Seraji and R. Colbaugh, "Force tracking in impedance control," *International Journal of Robotics Research*, vol. 16, no. 1, pp. 97–117, 1997.

[29] J. Duan, Y. Gan, M. Chen, and X. Dai, "Adaptive variable impedance control for dynamic contact force tracking in uncertain environment," *Robotics and Autonomous Systems*, vol. 102, pp. 54–65, 2018.

[30] M. Zheng, T. Yuan, and T. Huang, "Time-varying impedance control of port Hamiltonian system with a new energy-storing tank," *Complexity*, vol. 2018, Article ID 8134230, 10 pages, 2018.